International Journal of Extreme Manufacturing

PAPER • OPEN ACCESS

Triboelectric ‘electrostatic tweezers’ for manipulating droplets on lubricated slippery surfaces prepared by femtosecond laser processing

To cite this article: Jiale Yong *et al* 2024 *Int. J. Extrem. Manuf.* **6** 035002

View the article online for updates and enhancements.

You may also like

- Recent progress in bio-inspired macrostructure array materials with special wettability—from surface engineering to functional applications
Zhongxu Lian, Jianhui Zhou, Wanfei Ren et al.
- Magnetically maneuverable three-dimensional digital microfluidic manipulation of magnetic droplets for biochemical applications
Yuna Park, Kang Yong Lee, Taegyu Won et al.
- Femtosecond laser direct writing of functional stimulus-responsive structures and applications
Yuxuan Zhang, Dong Wu, Yachao Zhang et al.

This content was downloaded from IP address 42.3.25.129 on 08/03/2024 at 05:45

OPEN ACCESS
IOP Publishing | IMMT
International Journal of Extreme Manufacturing
Int. J. Extrem. Manuf. **6** (2024) 035002 (16pp)
https://doi.org/10.1088/2631-7990/ad2cdf

Triboelectric 'electrostatic tweezers' for manipulating droplets on lubricated slippery surfaces prepared by femtosecond laser processing

Jiale Yong[1,*], Xinlei Li[1], Youdi Hu, Yubin Peng, Zilong Cheng, Tianyu Xu, Chaowei Wang[*] and Dong Wu

CAS Key Laboratory of Mechanical Behavior and Design of Materials, Department of Precision Machinery and Precision Instrumentation, University of Science and Technology of China, Hefei 230027, People's Republic of China

E-mail: jlyong@ustc.edu.cn and chaoweiw@ustc.edu.cn

Received 6 October 2023, revised 22 December 2023
Accepted for publication 23 February 2024
Published 7 March 2024

Abstract

The use of 'Electrostatic tweezers' is a promising tool for droplet manipulation, but it faces many limitations in manipulating droplets on superhydrophobic surfaces. Here, we achieve noncontact and multifunctional droplet manipulation on Nepenthes-inspired lubricated slippery surfaces via triboelectric electrostatic tweezers (TETs). The TET manipulation of droplets on a slippery surface has many advantages over electrostatic droplet manipulation on a superhydrophobic surface. The electrostatic field induces the redistribution of the charges inside the neutral droplet, which causes the triboelectric charged rod to drive the droplet to move forward under the electrostatic force. Positively or negatively charged droplets can also be driven by TET based on electrostatic attraction and repulsion. TET enables us to manipulate droplets under diverse conditions, including anti-gravity climb, suspended droplets, corrosive liquids, low-surface-tension liquids (e.g. ethanol with a surface tension of 22.3 $mN{\cdot}m^{-1}$), different droplet volumes (from 100 nl to 0.5 ml), passing through narrow slits, sliding over damaged areas, on various solid substrates, and even droplets in an enclosed system. Various droplet-related applications, such as motion guidance, motion switching, droplet-based microreactions, surface cleaning, surface defogging, liquid sorting, and cell labeling, can be easily achieved with TETs.

Supplementary material for this article is available online

Keywords: triboelectric electrostatic tweezer, droplet manipulation, slippery surface, superhydrophobic surface, femtosecond laser

[1] These authors contributed equally.
[*] Authors to whom any correspondence should be addressed.

Original content from this work may be used under the terms of the Creative Commons Attribution 4.0 licence. Any further distribution of this work must maintain attribution to the author(s) and the title of the work, journal citation and DOI.

© 2024 The Author(s). Published by IOP Publishing Ltd on behalf of the IMMT
2631-7990/24/035002+16$33.00

1. Introduction

Controllable droplet manipulation is essential in a variety of applications, such as biological detection [1, 2], digital microfluidics [3–5], chemical reactions [6, 7], heat management [8, 9], water harvesting [10, 11], and printing technology [12, 13]. The contact operation carries the risk of contaminating the droplet and can easily cause volume loss due to liquid adhesion. Therefore, noncontact droplet manipulation is required in high-standard application scenarios. The existing methods of contactless droplet manipulation include passive and active methods [14, 15]. Passive methods rely on designing a geometric gradient structure, chemical gradient, or wettability gradient [16–19]. These gradients drive the droplet to move spontaneously in the direction of reduced system energy. However, droplet motion based on a gradient structure has inherent defects, such as short transport distances and poor flexibility [20, 21]. The tradeoff of hydrodynamics dictates that droplets can travel only a very short distance (usually in millimeters or centimeters) across gradient structures. Moreover, the droplets can only move spontaneously in a single direction, as determined by the gradient direction. Many active stimulus-driven methods, including magnetic field [22–24], electricity [25], light irradiation [26, 27], and acoustic field [3, 28] methods, have been developed to achieve more flexible and unlimited droplet manipulation. For example, adding magnetic particles to a droplet allows the droplet to be driven by an external magnetic field [29, 30]. However, additives also contaminate droplets, limiting the application of this method. Another method for magnetic manipulation is to prepare soft magnetic micropillars on the substrate [31–33]. Under the action of a magnetic field, the soft micropillars bend, causing the droplet to move forward. Similarly, when light-absorbing materials are embedded into a solid substrate, the resultant surface can efficiently convert the absorbed light into local heat [26]. The photopyroelectric effect triggered by light irradiation can generate a dielectrophoretic force within the droplet, allowing the light to drive the droplet. However, despite significant progress, these active stimulus-driven droplet manipulations must be carried out on specially designed substrates and cannot be extended to other materials. Therefore, developing an on-demand, noncontact, and substrate-independent method for manipulating droplets remains challenging.

Electrostatic attraction is a universal physical phenomenon. Figures 1(a)–(c) and movie S1 (supporting information) depict the effect of a positively charged glass rod with tribostatic electricity on a falling droplet. The droplet's fall is unaffected when the triboelectric charged rod (TCR) is far from the droplet (figure 1(a)). The positive and negative charges inside the droplet are randomly distributed (figure 1(d)). When the TCR approaches the falling droplet, the droplet deflects toward the rod due to the electrostatic force (F_e) applied to the droplet (figure 1(b)). Under the influence of the electric field generated by the TCR, the positive and negative charges inside the droplet are redistributed, with the negative charges gathering on the side near the rod and the positive charges gathering on the side away from the rod (figure 1(e)). The electrostatic attractive force acting on the droplet toward the rod is greater than the electrostatic repulsive force in the opposite direction, so the droplet is attracted and deflected in the direction of the rod. When the falling droplet is also positively charged according to the simple pressure-driven flow method [34, 35], the droplet deflects away from the rod (figure 1(c)) because the positively charged droplet is repelled by the electrostatic repulsion of the positive TCR (figure 1(f)). These experimental phenomena indicate that the static electricity generated from friction can exert electrostatic force on droplets, including both electrostatic attraction and repulsion. The combination of electrostatic interactions and liquid-repellent substrates provides us with an effective way to manipulate contactless droplets, as shown in figure 1(g). Dai *et al* controlled droplets to move and stop/pin on a superhydrophobic surface by electrostatic fields [36]. Jin *et al* prepared a droplet electrostatic tweezer (ET) using electrostatic force to manipulate various droplets [37]. The ET could remotely and programmatically trap or guide droplets on superhydrophobic surfaces. The reported electrostatic droplet manipulations are carried out mainly on lotus leaf-inspired superhydrophobic surfaces (figures 1(g-ii) and (g-iii)). However, the inherent limitations of superhydrophobic surfaces severely limit the range of applications of ET [38, 39]. First, the superhydrophobic surface has very little vertical adhesion to the liquid, so the droplet easily detaches from the solid surface. For example, in space without gravity or in some special applications where the material surface is downward, droplets cannot attach to superhydrophobic surfaces, so it is impossible to manipulate droplets on superhydrophobic surfaces. Second, in terms of stability, the Cassie state of a droplet on a superhydrophobic surface is prone to failure after suffering from an external force, vibration, or other interferences, resulting in the liquid droplet firmly adhering to the substrate. Third, the superhydrophobic surface may be wetted by low-surface-tension liquids other than water, preventing these liquids from being manipulated via ET on the superhydrophobic surface. Expanding the function and application range of ET in droplet manipulation is highly scientific and engineering important.

A liquid-repellent substrate is critical for electrostatic droplet manipulation. Without a base, the droplet's gravity would have to be balanced, adding complexity to the operation. Unlike superhydrophobic surfaces, Nepenthes-inspired lubricated slippery surfaces also have excellent liquid repellence and do not have the disadvantages of superhydrophobic surfaces (figure 1(g-iv)) [40, 41]. This slippery surface uses lubricant trapped between porous microstructures to form a layer of lubrication on the substrate surface to repel various liquids and has been successfully applied in various fields, such as droplet and bubble manipulation, cell engineering, biomedical, antifouling, anti-icing, and anticorrosion [39, 42–47]. By taking advantage of slippery surfaces, the realization of electrostatic manipulation of droplets by combining ET with slippery surfaces will open up many additional functions and applications (figure 1(g-v)).

Here, we use a triboelectric electrostatic tweezer (TET) to successfully achieve contactless, flexible, and precise droplet manipulation on lubricated slippery surfaces. Superhydrophobic surfaces and slippery surfaces are directly prepared by femtosecond laser processing. The manipulations of droplets on slippery surfaces and superhydrophobic surfaces with TET were compared. The droplets are driven to move by electrostatic forces as the charges inside the droplet are redistributed under TCR-generated electric fields. Electrostatic droplet manipulation can be applied under a variety of conditions and in various droplet-related applications, such as motion guidance, motion switching, droplet-based microreactions, surface cleaning, surface defogging, liquid sorting, and cell engineering.

2. Results and discussion

2.1. Preparation of the superhydrophobic surface and lubricated slippery surface

Figure 1(h) shows the process of preparing a superhydrophobic surface and a lubricated slippery surface in our experiment. A polydimethylsiloxane (PDMS) sheet with a thickness of 1 mm was chosen as the substrate because of its intrinsic hydrophobicity and excellent compatibility with silicone oils (the most commonly used lubricant). The characteristics of ultrashort pulse width and ultrahigh peak power have made femtosecond (10^{-15} s) lasers one of the most important tools in modern extreme and ultraprecision manufacturing [48–52]. Femtosecond laser processing was utilized to create the required microstructures on the PDMS surface, as shown in figure S2 (supporting information). After the laser treatment, uniform rough coral-like hierarchical micro/nanoscale structures were formed on the PDMS surface (figures 1(i) and S3 in the supporting information). There are abundant cracks and porous structures between the coral-like microstructures. Although slight oxidation and carbonization occur with laser ablation, the low-surface-energy C–H_3 and C–H_2 groups still dominate the ablated surface [53, 54]. Superhydrophobicity can be directly achieved after laser processing without any chemical modification (figures 1(h) and (i)). A water droplet on the resultant surface is spherical with a contact angle (CA) of (154.3 ± 2.1)° and can roll away easily at a sliding angle (SA) of (1.2 ± 0.8)° (figure 1(j) and movie S2 in the supporting information). A falling droplet can bounce multiple times on the resultant surface, indicating that the surface also has low vertical adhesion to the droplet (figures S4(a) and (b) and movie S2, supporting information). The vertical adhesive force between the structured surface and the water droplet was only (18.7 ± 4.7) μN (figure S4(c), supporting information). The excellent superhydrophobicity and ultralow water adhesion are ascribed to the synergistic effect of the inherent hydrophobicity of the PDMS substrate and the laser-induced rough surface microstructure. This synergistic effect allows the water droplet to touch only the top of the superhydrophobic microstructures (i.e. the so-called Cassie contact state) (figure 1(h-ii)) [55–57].

Lubricant infusion is needed to turn the laser-structured surface into a lubricated slippery surface. The lubricant used needs to have excellent electrical insulation so that it is not significantly changed by electrostatic interactions. As shown in figure 1(h-iii), electrically insulating silicone oil with a dielectric constant of ∼2.7 and a resistivity of 10^{11}–10^{12} Ω·m was used as the lubricant and poured onto the PDMS surface. Since silicone oil molecules have a chemical structure similar to that of cross-linked PDMS, they can not only fill between the rough microstructures of the PDMS surface but also partially penetrate the PDMS network [58]. This excellent compatibility allows the silicone oil to be firmly locked into the PDMS substrate. When the excess oil is removed, a smooth and ultrathin lubricant layer is formed on the PDMS surface. The water droplets are nearly hemispherical with a CA of 95.4 ± 1.8° on such a lubricated slippery surface (figure 1(k)). Despite the large contact area between the droplets and the slippery surface, their lateral adhesion is very small. Figure 1(l) and movie S3 (supporting information) show that a water droplet slides down on the slippery surface at a tilt angle of 5° (the average SA of the droplet on the slippery surface is only 0.8°). The slippery surface also exhibited excellent liquid repellence because the trapped lubricant layer prevents the droplet from making effective contact with the solid substrate (figure 1(h-iv)).

2.2. Droplet motion driven by TETs

The manipulations of liquid droplets on the superhydrophobic surface and lubricated slippery surface by TET were compared. A glass rod with a diameter of approximately 7 mm becomes positively charged when rubbed against the silk. The TCR is moved close to the droplet until the droplet begins to move. The manipulation of droplets with a volume of 10 μl on superhydrophobic surfaces is shown in the supporting information (including the description and figure S1). The droplet rolling speed is particularly fast under electrostatic attraction, even above 100 mm·s^{-1}. It takes only 137 ms for the droplets to start moving and attach to the TCR (movie S4, supporting information). Such swift motion makes the droplets difficult to control. In addition to moving in the direction parallel to the surface, we also try to move the TCR from an oblique height closer to the droplet. Unfortunately, the droplet can easily separate from the superhydrophobic surface and fly toward the high-altitude TCR because of the very low adhesion of superhydrophobic surfaces to water droplets in the direction perpendicular to the substrate surface (movie S5, supporting information). The small adhesive force cannot resist the electrostatic force in the vertical direction. When a negatively charged water droplet was previously placed on the superhydrophobic surface and a positive TCR gradually approached the droplet, the droplet became deformed but firmly adhered to the surface. This reveals that the droplet is difficult to move, even though the electrostatic force on the charged droplet is stronger than that on the neutral droplet. The negatively charged droplet can induce positive charges on the surface of the PDMS substrate due to electrostatic induction. The attractive electrostatic force of the polar opposite charges exerts a downward

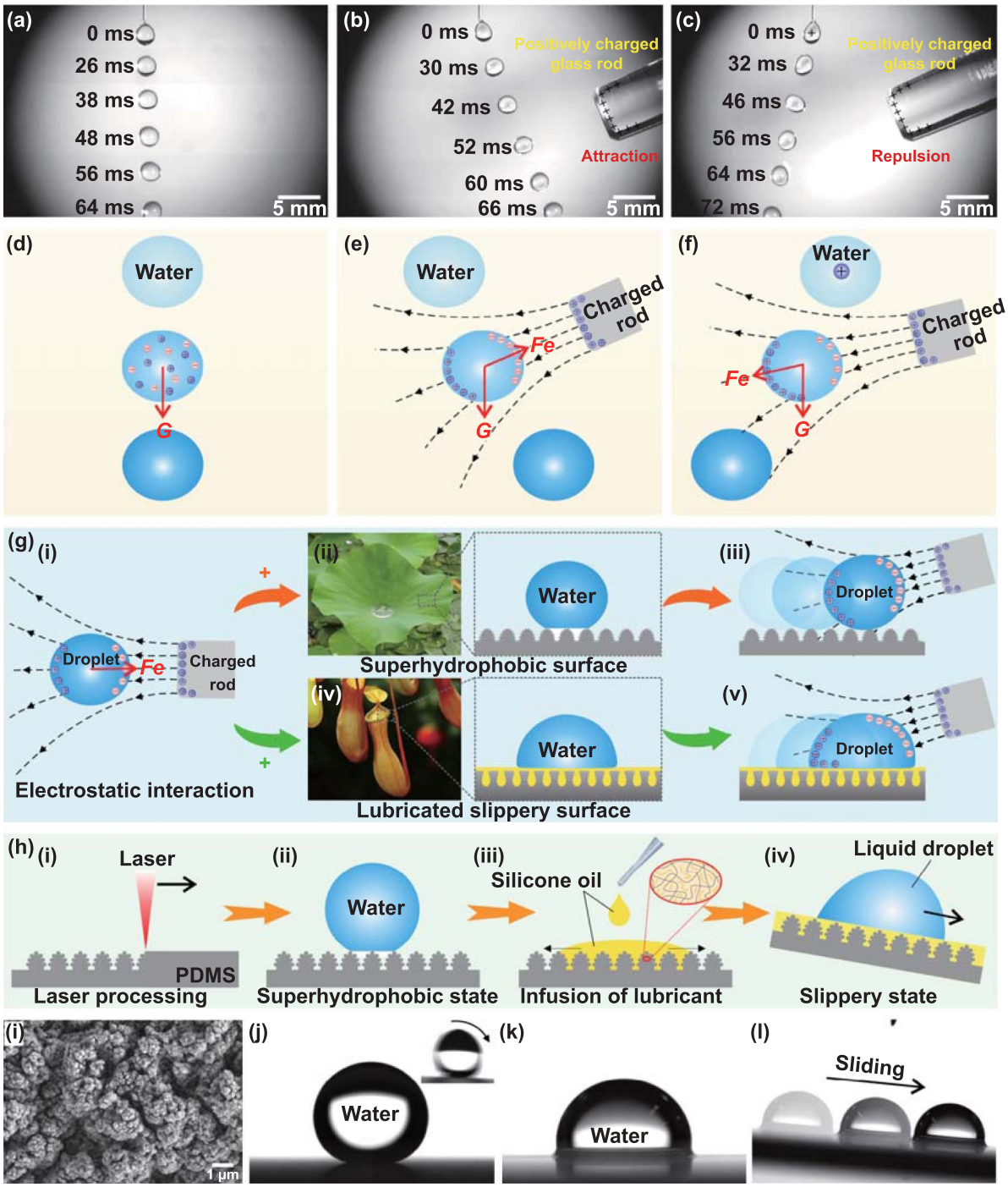

Figure 1. The effect of frictional static electricity on droplets and the idea of manipulating a droplet on liquid-repellent substrates based on electrostatic interactions. (a)–(c) Influence of a positive TCR on the falling process of water droplets: (a) the TCR is far from the droplet, (b) the TCR moves close to the falling water droplet, and (c) the falling droplet is positively charged and the TCR is close to the falling droplet. (d)–(f) Schematic diagram of the electrostatic influence on the motion of falling droplets corresponding to (a)–(c), respectively. (g) Schematic diagram of manipulating droplets by combining electrostatic interaction and liquid-repellent substrates: (i) the electrostatic attraction of TCR to a neutral liquid droplet, (ii) the photo of the superhydrophobic lotus leaf and the contact state between a water droplet and superhydrophobic microstructure, (iii) driving a droplet to roll forward on the superhydrophobic surface by electrostatic interaction, (iv) the photo of the slippery Nepenthes and the contact state between a water droplet and lubricated slippery surface, and (v) driving a droplet to slide forward by electrostatic interaction on a lubricated slippery surface. (h) Preparation of the superhydrophobic surface and the lubricated slippery surface by femtosecond laser microfabrication: (i) ablation of the PDMS surface by a laser, (ii) droplet on the resultant superhydrophobic microstructure, (iii) infusion of lubricant (silicone oil) into the rough laser-structured PDMS surface, and (iv) liquid repellence of the lubricated slippery surface. (i) Morphology of the PDMS surface after laser ablation. (j) Shape of a droplet on the superhydrophobic PDMS surface. The inset shows a snapshot of the rolling process of the droplet on the inclined surface at a tilt angle of 1.2°. (k) Water droplet on the as-prepared lubricated slippery surface. (l) Time-lapse trajectory of a droplet sliding on a lubricated slippery surface at a tilt angle of 5°.

pull on the liquid surface near the solid surface, causing the droplet to partially penetrate into the rough surface microstructure. Therefore, the charged droplets strongly adhered to the superhydrophobic surface (figure S5, supporting information) because the charged droplets were in the highly adhesive Cassie–Wenzel transition state [57]; thus the charged droplets were not easily moved by electrostatic interactions. Therefore, there are many limitations to manipulating droplets on superhydrophobic surfaces by TET.

The characteristics of a lubricated slippery surface can easily eliminate the abovementioned difficulties associated with superhydrophobic surfaces. Figure 2(a) and movie S4 (supporting information) show the motion of a 10 μl neutral water droplet on the lubricated slippery surface attracted by a +5.5 kV charged glass rod. The changes in droplet position and velocity with time are depicted in figure 2(b). The distance (d) between the droplet and the TCR gradually decreases with time as the droplet approaches the charged rod. The droplet initially slides at a very low velocity (v), approximately moving forward at a constant speed. However, when approaching the near-glass rod, v suddenly increases. This motion process can also be reflected in the relationship between the droplet motion velocity/acceleration and d (figure 2(c)). The results also reveal that the closer the droplet is to the TCR, the more attractive it is. There is a critical distance, d_0, between the droplet and the TCR, which allows the droplet to overcome the adhesion of the substrate and begin to move. Figure 2(d) shows the measured results of d_0 under the different electrostatic potentials of the TCR. d_0 is positively correlated with the applied potential of frictional static electricity on the TCR within the error range. A higher potential results in a larger d_0, so the control distance can be longer; in other words, a larger electrostatic potential can manipulate droplets farther away. For droplets of different volumes, d_0 increases with increasing droplet volume when the volume is less than 10 μl (the droplets can be considered approximately spherical because their diameters are smaller than the capillary length) and roughly reaches saturation for larger droplets (the droplet deformation is quite serious), as shown in figure 2(e).

In contrast to a superhydrophobic surface, a lubricated slippery surface has high adhesion to droplets in the vertical direction, although the adhesion is still low in the lateral direction [59]. The vertical adhesion ensures that the droplets cannot break away from the slippery surface. As shown in figure 2(f) and movie S5 (supporting information), when a TCR is gradually moved to approach the water droplet from above, the droplet always stays on the solid surface, although the droplet is stretched upward due to electrostatic attraction. Even when the distance between the rod and the droplet reaches the minimum limit at which an electrical discharge occurs, the water droplet remains on the slippery surface. The vertical adhesion between droplets and slippery surfaces makes it possible to manipulate droplets without gravity. For example, in a space station, astronauts or scientists can use electrostatic forces to move droplets on a lubricated slippery surface without separating the liquid droplets from the solid surface or flying into the air.

The contact state between the droplet and slippery surface is very different from that of Cassie contact on superhydrophobic surfaces, which relies on the air cushion trapped beneath the droplet [41, 57]. The space between the droplet and the solid surface is filled with lubricant on a slippery surface, stabilizing this contact state. The contact state is not changed by pressure, disturbance, or even charging of the droplet. Electrostatic forces can also drive charged droplets to slide on a slippery surface. When the charges of the TCR have the opposite polarity to the charges carried by the droplet, the TCR attracts the droplet to move (figure 2(g)). In contrast, when the TCR is charged to the same polarity as the droplet, the charged rod repels the droplet (figure 2(h)). For example, figure 2(i) shows the process of a negatively charged droplet being attracted (pulled) forward by a positive TCR, and figure 2(j) shows the process of a positively charged droplet being repelled (pushed) forward on a lubricated slippery surface by a positive TCR. Notably, negative TCRs can also achieve droplet manipulation on a slippery surface (figure S6, supporting information).

The TCR can directly and remotely exert force on droplets, similar to tweezers, to move a droplet on a slippery surface. This technique for droplet manipulation can be specifically referred to as 'triboelectric electrostatic tweezers (TETs)'.

2.3. Mechanism of electrostatic droplet manipulation

The charges on the TCR generate an electrostatic field around the rod, as shown in figure 2(k). When an electrostatic field is applied to a droplet, electrostatic induction will cause redistribution of the charges in the droplet, i.e. the polarization process [37, 60–62]. The induced charges contribute to the electrostatic Coulomb force between the droplet and the TCR. The electrostatic force, $\boldsymbol{F}_e$, acting on an object is the sum of the Maxwell stress working on the surface of the object, and such a surface force is the integral of the surface of the object. For a liquid droplet under an electrostatic field, the electrostatic force can be expressed as [63, 64]:

$$\boldsymbol{F}_e = \oint \left[\varepsilon \boldsymbol{E}(\boldsymbol{E}\boldsymbol{n}) - \frac{\varepsilon}{2}\boldsymbol{E}^2\boldsymbol{n}\right] \mathrm{d}S \tag{1}$$

where ε is the permittivity of the droplet ($\varepsilon = \varepsilon_r\varepsilon_0$, ε_r is the relative permittivity of the liquid, and ε_0 is the permittivity of air), $\boldsymbol{E}$ is the electric field intensity, $\boldsymbol{n}$ is the surface unit normal, and S is the surface area of the droplet. The Coulomb force can be quantified by the following formula in tensor form [37, 65, 66]:

$$\begin{aligned} &\boldsymbol{F}_e = \oint T_{e,ij} \cdot \boldsymbol{n} \mathrm{d}S, \\ &\text{with } T_{e,ij} = \varepsilon_0 \left(E_i E_j - \frac{\delta_{ij}}{2}E^2\right), i,j = x,y,z \end{aligned} \tag{2}$$

where $\boldsymbol{T}_e$ is the Maxwell stress tensor applied on the droplet, δ_{ij} is the Kronecker delta function, and E is the magnitude of the electric field intensity. The distributions of $\boldsymbol{T}_e$ in the lateral direction (T_x) and vertical direction (T_z) can be calculated through finite-element analysis using COMSOL Multiphysics

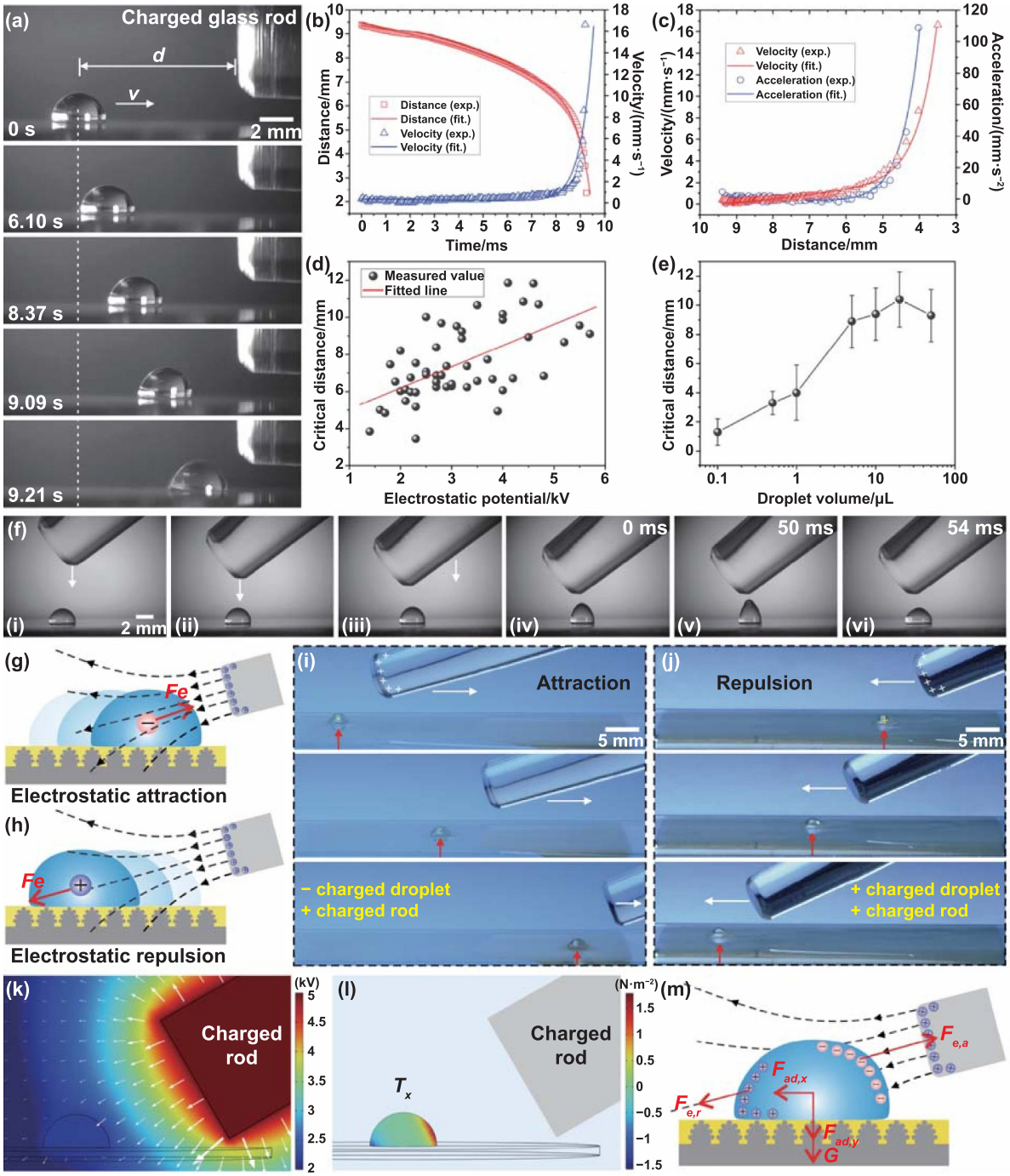

Figure 2. Droplet motion on the lubricated slippery surface driven by electrostatic interaction. (a) A neutral water droplet sliding toward a positively charged glass rod with a surface potential of +5.5 kV. (b) Variation in the distance between the droplet and the TCR and the motion velocity with time. (c) The velocity and acceleration of the droplet at different distances from the TCR. (d) Influence of the electrostatic potential of the TCR on the critical distance allowing the droplet to begin to move (at a droplet volume of 10 μl). (e) Influence of the droplet volume on the critical distance (at a surface potential of +5 kV). (f) Process of bringing a TCR from above close to the droplet on the lubricated slippery surface. As the TCR gradually approaches the water droplet, the droplet is stretched upward due to electrostatic attraction, and finally, electrical discharge occurs (steps iv–vi). (g) and (h) Schematic diagram of the electrostatic interaction between the TCR and the charged droplets on the lubricated slippery surface: (g) attractive interaction and (h) repulsive interaction. (i) Process of a negatively charged droplet being attracted (pulled) forward by a positive TCR. (j) Process of a positively charged droplet being repelled (pushed) forward by a positive TCR. (k) Numerical simulation (based on finite element analysis) of the electric potential distribution around the TCR with a surface polarization voltage of +5 kV. The white arrows indicate the direction and magnitude of the electric field strength. (l) Distribution of the Maxwell stress tensor exerted on the droplet in the lateral direction (T_x). (m) Force analysis of droplets on the liquid-repellent surface under electrostatic interactions.

simulation, as shown in figures 2(l) and S7 (supporting information), respectively.

Taking a positively charged rod as an example, under the influence of the electrostatic field generated by the TCR, the induced negative charges gather on the droplet surface near the TCR because of electrostatic equilibrium. In contrast, the positive charges gather on the side farthest from the TCR. Therefore, the electrostatic force on the droplet consists of two parts ($\boldsymbol{F}_e = \boldsymbol{F}_{e,a} + \boldsymbol{F}_{e,r}$): the attraction force ($\boldsymbol{F}_{e,a}$) on the negative charges and the repulsion force ($\boldsymbol{F}_{e,r}$) on the positive charges (figure 2(m)). Although the charges are not uniformly distributed, we can treat them as a point charge for simplicity, with a total charge of q. The polarization charge due to electrostatic induction can be written as [20, 62]:

$$q = (\varepsilon_r - 1)\,\varepsilon_0\,|\nabla \boldsymbol{E}|\,. \tag{3}$$

According to Coulomb's law, the net electric force can be approximated as:

$$\boldsymbol{F}_e = \boldsymbol{E}q = (\varepsilon_r - 1)\,\varepsilon_0\,|\nabla \boldsymbol{E}|\boldsymbol{E} \tag{4}$$

where $\boldsymbol{E} = -\nabla V$ (V is the electric potential). The intensity and variation of the electric field are depicted in figure 2(k). The further away the charged rod is, the smaller the electric potential and the smaller electric field strength. Therefore, the attraction where the negative charges accumulate is greater than the repulsion at the side where the positive charges accumulate. That is, the attraction of the negatively induced charges (near the TCR) to the droplet is dominant (figure 2(l)). The direction of the resultant electrostatic force on the droplet is toward the TCR. This electrostatic force provides the driving force for droplet motion.

The dynamic behaviors of droplets on slippery surfaces are determined by the resultant force acting on the droplet. As shown in figure 2(m), there are four main forces acting on the droplet: the electrostatic Coulomb force (F_e), the gravitational force of the droplet ($G = mg$, where m is the mass of the droplet and g is the acceleration of gravity), the lateral adhesive force ($F_{ad,x}$), and the vertical adhesive force ($F_{ad,z}$). We only consider lateral droplet manipulation. The horizontal composition of the electrostatic force and lateral adhesive force could be responsible for the propulsive movement of droplets on a horizontal surface. The net force F driving the droplet can be expressed as:

$$F = F_e\cos\alpha - F_{ad,x} \tag{5}$$

where α is the angle between the electrostatic force and the horizontal direction. This relation provides a fundamental understanding of droplet motion in an electrostatic field. The lateral adhesive force can be expressed as $F_{ad,x} = kw\gamma\,(\cos\theta_r - \cos\theta_a)$, where k, w, γ, θ_r, and θ_a are the shape correction coefficient, width of the droplet, surface tension of the droplet, receding CA, and advancing CA, respectively [67, 68]. Since slippery substrates have very little lateral adhesive force to water droplets, when the TCR is close enough to the droplet, F_e can be greater than $F_{ad,x}$. When $F > 0$, the droplet begins to move, which is driven forward by electrostatic forces. When the droplet slides on a surface lubricated by silicone oil, it will be affected by motion resistance, mainly caused by viscous force (F_μ). According to the experimental results of Aizenberg *et al*, F_μ can be approximated as [69–71]:

$$F_\mu \sim \pi\gamma_{wo}RCa^{2/3} \tag{6}$$

where γ_{wo} is the water–oil interfacial tension, R is the droplet radius, and Ca is the capillary number $Ca = \mu_0 v/\gamma_{wo}$ (μ_0 is the oil viscosity and v is the motion velocity of the droplet). Thus, the equation of motion of the droplet can be described as follows:

$$F_e\cos\alpha - F_\mu = ma = m\frac{dv}{dt} \tag{7}$$

where a is the acceleration of the droplet and t is the time. Therefore, by moving the charged rod and maintaining the proper distance between the droplet and the rod, the droplet can be guided to move uniformly on the slippery surface. The motion velocity can be adjusted from low to high by controlling the proper distance from the rod.

2.4. Multifunctional droplet manipulation with ETs

The characteristics of the lubricated slippery surface enable the TET to have the dexterous ability to manipulate droplets. Figure 3(a) and movie S6 (supporting information) show that a 10 μl water droplet attracted by a TCR slides upward along the inclined slippery surface. Due to the vertical adhesion of the slippery surface to liquid droplets, the droplets will not fall off the slippery surface even if the surface is turned over. This property allows TETs to manipulate suspended droplets. Suspended droplets can also be attracted remotely through electrostatic interactions (figure 3(b) and movie S6 in the supporting information). In contrast, manipulating suspended droplets on superhydrophobic surfaces is impossible because droplets cannot hang on superhydrophobic surfaces. The electrostatic repulsion between a TCR and a charged droplet of the same polarity can push a tiny droplet to climb vertically against gravity on a vertical slippery surface (figure 3(c) and movie S6 in the supporting information).

In addition to water, electrostatic forces can manipulate a variety of other liquids on slippery surfaces. For example, common fluids (e.g. milk, coffee, cola, and juice) during life are repelled by slippery surfaces and thus can be easily moved with the TCR (figure S8 and movie S7, supporting information). The slippery surface is resistant to corrosion because the lubricant layer can prevent corrosive liquids from effectively contacting the substrate surface [72]. Therefore, the manipulation of corrosive droplets is allowed on slippery surfaces. As shown in figure 3(d) and movie S7 (supporting information), corrosive droplets composed of acid HCl solution at pH = 2 (figure 3(d-i)), alkali NaOH solution at pH = 12 (figure 3(d-ii)), and 10% NaCl salt solution

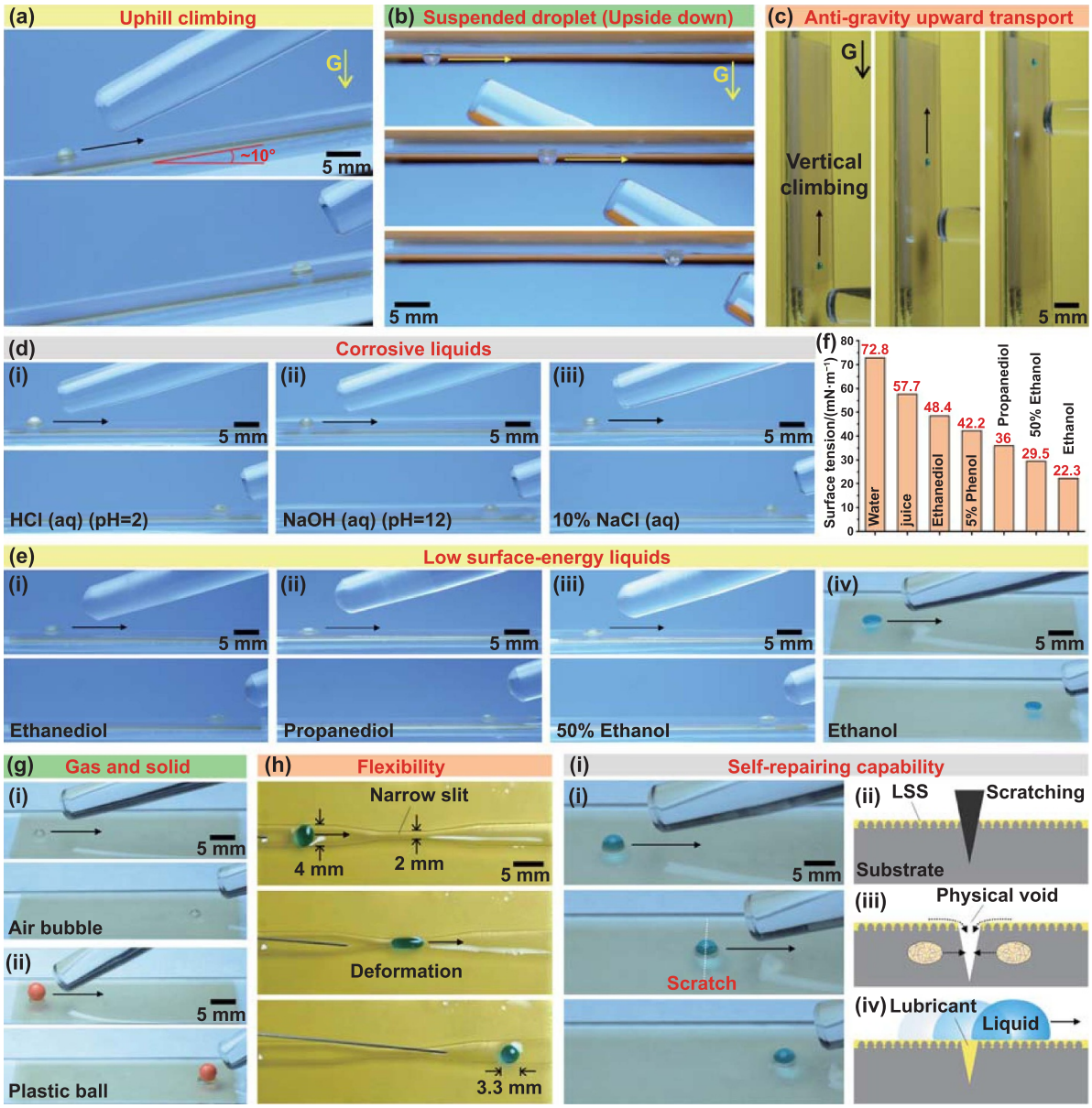

Figure 3. Multifunctional manipulation of droplets by triboelectric electrostatic tweezers. (a) Water droplets sliding upward along the slippery surface at a tilt angle of 10°. (b) Moving a suspended droplet with the slippery surface turned over. (c) Pushing a 1 μl charged droplet to climb vertically against gravity on the vertical surface by electrostatic repulsion. (d) Manipulating corrosive droplets on slippery surfaces: (i) HCl solution (pH = 2), (ii) NaOH solution (pH = 12), and (iii) 10% NaCl solution. (e) Manipulating liquid droplets with low surface tension on slippery surfaces: (i) ethanediol, (ii) propanediol, (iii) 50% ethanol, and (iv) ethanol. (f) The surface tensions of the liquids measured in our experiment. (g) Motion of a (i) gas bubble and (ii) plastic ball on the slippery surface attracted by a TCR. (h) Process of a positively charged droplet being remotely pushed to pass through a slippery narrow slit by a positively charged metal rod. (i) A droplet is attracted to slide smoothly across a scratch damaged by a knife: (i) process of droplet sliding through the scratch and (ii)–(iv) mechanism of the self-repairing capability of the slippery surface.

(figure 3(d-iii)) can be driven to slide by electrostatic interactions. The slippery surface is also able to repel low-surface-tension liquids, so droplets with low surface tension, such as ethanediol (figure 3(e-i)), propanediol (figure 3(e-ii)), 50% ethanol (figure 3(e-iii)), and ethanol (figure 3(e-iv)), can also be transported on the slippery surface (movie S7 in the supporting information). The surface tension of these droplets is as low as 22.3 $mN{\cdot}m^{-1}$ (figure 3(f) and table S1 in the supporting information). In contrast, due to Cassie contact state failure, superhydrophobic surfaces are usually wetted by liquids with low surface tension (figure S9, supporting information), preventing these liquids from being moved by electrostatic forces on superhydrophobic surfaces. Surprisingly, in addition to liquids, small air bubbles (figure 3(g-i)) and solid plastic balls (figure 3(g-ii)) can also be attracted by the TCR to move forward on the slippery surface (movie S8, supporting information). Induced charges are also generated on the surfaces of the bubbles and the solid balls, causing the bubbles

and plastic balls to move under the action of electrostatic forces.

The deformability of fluids allows droplets to pass through narrow slits. Figure 3(h) and movie S9 (supporting information) show the process of a positively charged 20 μl droplet being remotely pushed through a slippery narrow slit with a width of 2 mm by a positively charged metal rod. The bottom and sidewalls of the slit are composed of femtosecond laser-structured slippery microstructures. The bottom diameter of the droplet on the slippery surface is approximately 3.3 mm, which is less than the width of the narrow slit. When the droplet entered the slit, it elongated and squeezed in the slit. Finally, the droplet successfully passed through the narrow slit whose width is 1.7 times smaller than the droplet diameter. This flexibility allows the droplet to act as a soft robot that can be controlled remotely by a TET to perform specific tasks in a confined space.

A slippery surface usually has high stability and good self-repairing capability [41]. Even if subjected to multiple bending, friction, and droplet scour treatments, the slippery surface prepared by the femtosecond laser can maintain liquid repulsion for a long time [41, 44]. As shown in figure 3(i-i) and movie S10 (supporting information), even if a knife scratches the slippery surface, the TCR can guide liquid droplets to slide over the scratch. This outstanding performance is due to the spontaneous repair of the damaged area by the lubricant (figures 3(i-ii)–(i-iv)). The lubricant on the slippery surface and the lubricant filled inside the PDMS network quickly flowed to the damaged area and filled the scratches (figure 3(i-iii)), ensuring the smoothness of the surface lubricant layer. Thus, the damaged area still allows the droplet to slide through (figure 3(i-iv)). In contrast, droplets stick to scratches on superhydrophobic surfaces because of the high adhesion of the damaged area to the liquid (figure S10, supporting information).

In addition to PDMS, slippery surfaces can be prepared on various substrates, such as polytetrafluoroethylene (PTFE), aluminum, silicon, and glass. As shown in figure S11 and movie S11 (supporting information), droplets can also be manipulated on these slippery substrates by TET. The substrates include both electrically conductive and electrically insulating materials. The successful movement of droplets on different substrates demonstrated that electrostatic droplet manipulation on slippery surfaces is a universal method and does not depend on the type of solid substrate.

TETs not only enable contactless, flexible, and precise droplet manipulation on slippery surfaces but also exhibit many dexterity capabilities. As shown in table 1, manipulating liquid droplets on a slippery surface based on a TET has many advantages over manipulating liquid droplets on a superhydrophobic surface.

Table 1. Comparison of electrostatic droplet manipulation on superhydrophobic surfaces and lubricated slippery surfaces. '√' and '×' denote 'can' and 'connot', respectively.

Content	Superhydrophobic surface	Lubricated slippery surface
Droplet motion velocity	Too fast (uncontrollably)	Slow (easy to control)
In a weightless environment (e.g. in the space station)	× (droplets separating from substrate)	√
Charged droplets	Difficulty (increased adhesion between droplets and surfaces)	√ (electrostatic attraction or repulsion)
Inverted/upright substrate (e.g. suspended droplet)	× (droplets separating from substrate)	√
Corrosive liquids	Not sure (only durable surface can)	√
Liquids with low surface tension (e.g. 22.3 $mN{\cdot}m^{-1}$ for ethanol)	×	√
Crossing over the damaged area (i.e. the self-repairing ability of surface)	×	√
Both electrically conductive and insulating substrates	√	√

2.5. Diverse applications of electrostatic droplet manipulation

The remote and flexible manipulation of droplets with TETs enables various practical applications ranging from motion guidance, motion switching, droplet-based microreaction, surface cleaning and surface defogging to liquid sorting. For example, a droplet on a slippery surface can be dragged remotely in any direction under electrostatic attraction by a TCR. TET can even guide droplets out of complex maze patterns, as shown in figure 4(a) and movie S12 (supporting information). Small droplets can carry chemical reagents. Contact between different droplets can trigger reactions between different chemical reagents, also known as droplet microreactions. Figure 4(b-i) and movie S13 (supporting information) show the process of guiding a 10 μl aqueous droplet of $AgNO_3$ to merge with a $FeCl_3$ droplet on a slippery surface. When the two droplets come into contact, a precipitation reaction ($Ag^+ + Cl^- \rightarrow AgCl\downarrow$) occurs, forming a white precipitate inside the merged droplet (figure 4(b-ii)). As the merged droplet continues to move and comes into contact with another phenol droplet, the newly merged droplet turns purple because of the color reaction ($6C_6H_5OH + Fe^{3+} \rightarrow [Fe(C_6H_5O)_6]^{3-} + 6H^+$) (figure 4(b-iii)). It should be noted that the reaction can also be carried out by moving the phenol droplet to other droplets. Both inorganic and organic reactions based on droplet manipulation have been demonstrated on slippery surfaces. In contrast, achieving an organic droplet reaction on a superhydrophobic surface is difficult because low-surface-tension organic

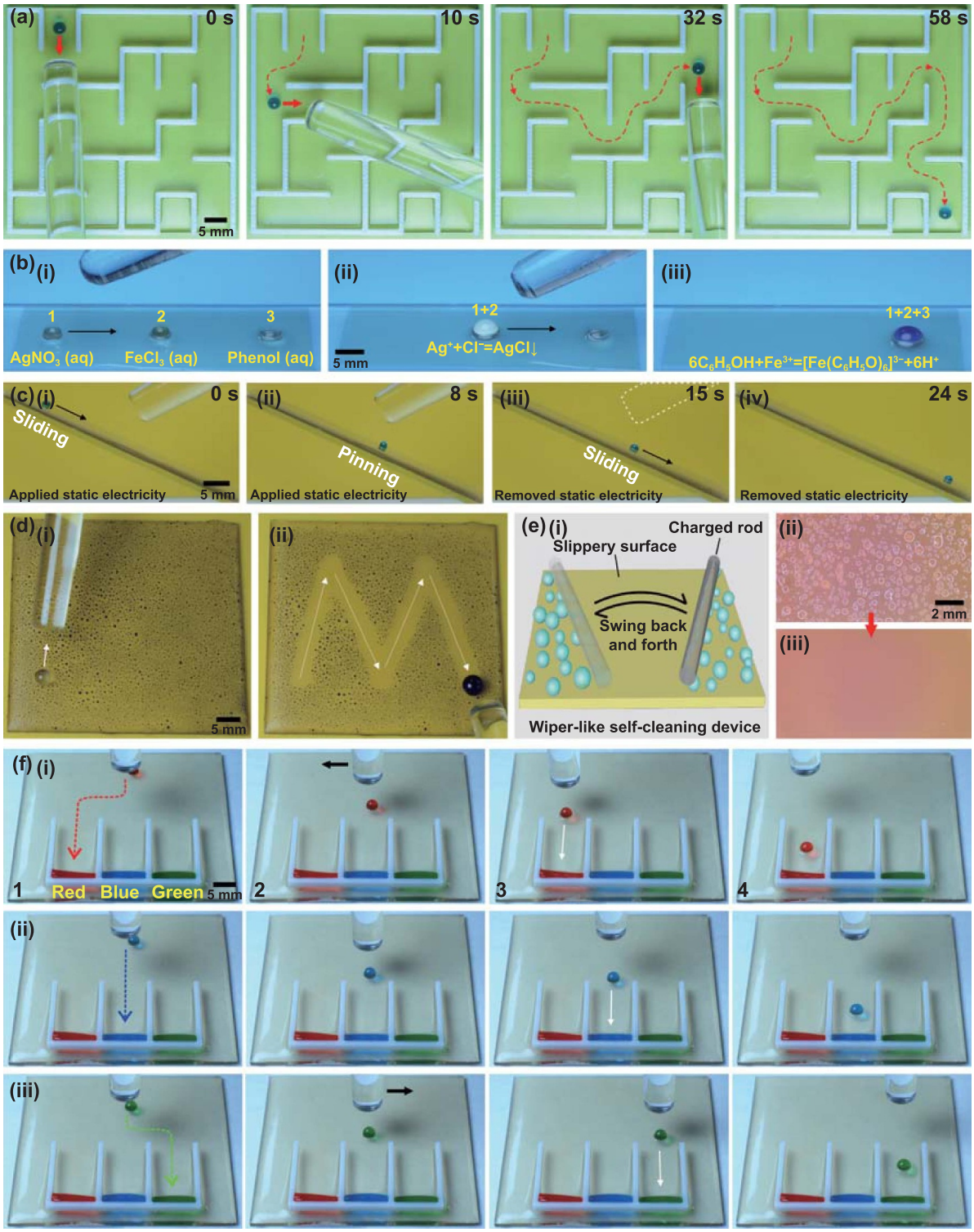

Figure 4. Diverse applications of electrostatic droplet manipulation. (a) Sequential images of remotely guiding a droplet through a complex maze pattern by a TCR. (b) Achievement of droplet-based chemical microreaction by the electrostatic manipulation of droplets: (i) moving droplet-1 ($AgNO_3$ solution) toward droplet-2 ($FeCl_3$ solution), (ii) precipitation reaction between droplet-1 and droplet-2 and further moving the merged droplet toward droplet-3 (phenol solution), and (iii) the color reaction after all the droplets merge. (c) Motion switch to control the sliding and pinning states of droplets on a slippery surface: (i) the droplet slides down by gravity, (ii) the droplet stops by the electrostatic attraction of the TCR, and (iii) and (iv) the droplet continues to slide down after the TCR is removed. (d) Cleaning the contaminants on the slippery surface by the TET-guided liquid droplet: (i) tiny spray drops as contaminants on the surface and (ii) a cleaning droplet guided to slide along an 'M'-shaped route by a TCR. (e) Wiper-inspired surface defogging: (i) schematic drawing of the defogging device where a charged rod swung side to side over the slippery surface, (ii) optical image of tiny fog drops on the surface before fog removal, and (iii) optical image of the surface after defogging. (f) Liquid sorting by guiding different droplets to different sliding routes: (i) red droplets, (ii) blue droplets, and (iii) green droplets distributed to the left, middle, and right collection tanks, respectively.

liquids (e.g. phenol) usually wet the surface (figure S12, supporting information). The TET can be used for motion switching to control the sliding and pinning state of the droplet on a slippery surface, as shown in movie S14 (supporting information). When a TCR is suspended above the slippery surface, droplets sliding on the surface by gravity stop below the TCR due to electrostatic attraction (figures 4(c-i) and (c-ii)). The droplet is pinned on the slippery surface without the TCR touching it directly. Once the TCR is removed, the droplet will continue sliding downward (figures 4(c-iii) and (c-iv)). Therefore, droplet motion can be remotely switched between sliding and pinning states in a noncontact manner.

There are no restrictions on the direction or travel distance for electrostatic droplet manipulation, which makes it possible to remotely and precisely clean contaminants on a slippery surface with a TET. When the droplet slides forward, foreign objects on the surface can be picked up. As shown in figure 4(d) and movie S15 (supporting information), a slippery surface contaminated with tiny spray drops is cleaned by a large droplet guided by a TCR. The clean droplet is driven to slide along an 'M'-shaped route, during which all contaminants are removed (figure 4(d-ii)). By controlling the motion of the droplets, the cleaning path can be precisely programmed. Inspired by the windshield wiper, the charged rod swung from side to side to clean fog drops on the slippery surface without direct contact (figure 4(e-i)). Tiny droplets are attracted to both sides of the slippery surface, keeping the surface clear (figures 4(e-ii) and (e-iii)).

Under the electrostatic attraction of a TCR, different droplets can be guided to different sliding routes remotely to achieve liquid sorting (movie S16, supporting information). As shown in figure 4(f) and figure S13 (supporting information), a droplet can slide down slowly by gravity on an inclined slippery surface (step-1). When the droplet reaches the vicinity of the TCR, the height of the TCR is decreased to generate a stronger electrostatic force on the droplet (step-2). Then, if the TCR is moved laterally, the droplet will move with it (step-3). Once the droplet slides to the designated route, the TCR will be lifted to reduce electrostatic attraction. After that, the droplet continues to slide downward and toward the liquid collection zone (step-4). Figures 4(f-i) shows the process of a red droplet being assigned to the left collection tank via electrostatic interactions. Following the same process, blue and green droplets were distributed to the middle and right collection tanks, respectively (figures 4(f-ii) and (f-iii)).

2.6. Mechanically assisted vertical electrostatic tweezers (VETs)

The TET can be assembled into a mechanical control system to achieve more accurate control of droplets. As shown in figure 5(a), the TCR is vertically fixed on a three-dimensional mobile platform. As the TCR moves directly above the droplet and then decreases to a suitable height, the droplet will be bound by the electrostatic force. When the TCR moves laterally, the droplets on the slippery surface will move with it, always under the rod (figure 5(b)). It is like manipulating droplets with a VET. Figure 5(c) reveals the underlying mechanism of the ability of the VET to move droplets. The electrostatic force acting on the droplet directly below the TCR is symmetric in the horizontal plane; thus, there is no lateral force on the droplet (figures 5(c-i) and (c-ii)). Once the TCR is moved forward and the droplet is not directly below the TCR, the electrostatic force on the droplet will be asymmetrical in the horizontal plane and stronger along the center of the rod (figures 5(c-iii) and (c-iv)). The asymmetrical electrostatic force pointing to the TCR will drive the droplet to slide to a position directly below the TCR, again achieving horizontal electrostatic symmetry. As a result, the droplet is always below the TCR and can be moved remotely by the VET. The control strength of the VET is affected by the distance between the TCR and the droplet. When the distance between the TCR and the droplet is close, the droplet deformation is more serious, indicating that the VET strongly binds the droplet (figure 5(d)). A strong binding force can accelerate droplet manipulation. However, too small a distance can easily lead to disruptive discharge. By mechanically moving the TCR horizontally, the droplet can slide back and forth on the slippery surface (figure 5(e) and movie S17 in the supporting information). It should be noted that there is a small position delay between the droplet and the rod during droplet movement because the motion of the droplet is affected by viscous resistance (figure 5(f)). The measured displacement delay and time delay are 2.1 mm and 1.0 s, respectively, at a velocity of 2 $mm{\cdot}s^{-1}$. Despite the motion delay, the droplet can eventually reach the position directly below the rod, meaning that it can obtain its target position precisely.

VET strongly binds droplets, so droplets of different volumes can be manipulated (movie S18, supporting information). As shown in figure 5(g), even water droplets much smaller in diameter than the TCR (e.g. a 100 nl water droplet) or enormous pie-shaped droplets (e.g. a 0.5 ml water droplet) can be transported by the VET. Unlike other reported methods of droplet manipulation that require a predetermined pathway [73, 74], the guided mode of mechanically assisted VET allows the droplet to move in any desired direction. Figure 5(h) and movie S19 (supporting information) show the use of the VET to remotely move a droplet along a handwritten Chinese character-shaped track (meaning 'happy') on a slippery surface. The droplet faithfully followed the tweezers. By controlling the mobile platform through a computer program, we can more precisely control or design the motion path of the droplets. In addition, compared with reported ETs with ultrahigh applied voltages [37], TETs based on frictional static electricity are safer and more portable.

The ability of the VET to remotely transport droplets allows us to manipulate liquids in an enclosed system, as shown in figure 5(i-i). As a demonstration, a water droplet on the slippery surface was placed into a disposable Petri dish (the most common cell culture plate) and covered. We succeeded in moving the droplet from outside the closed system (figure 5(i-ii) and movie S20 in the supporting information).

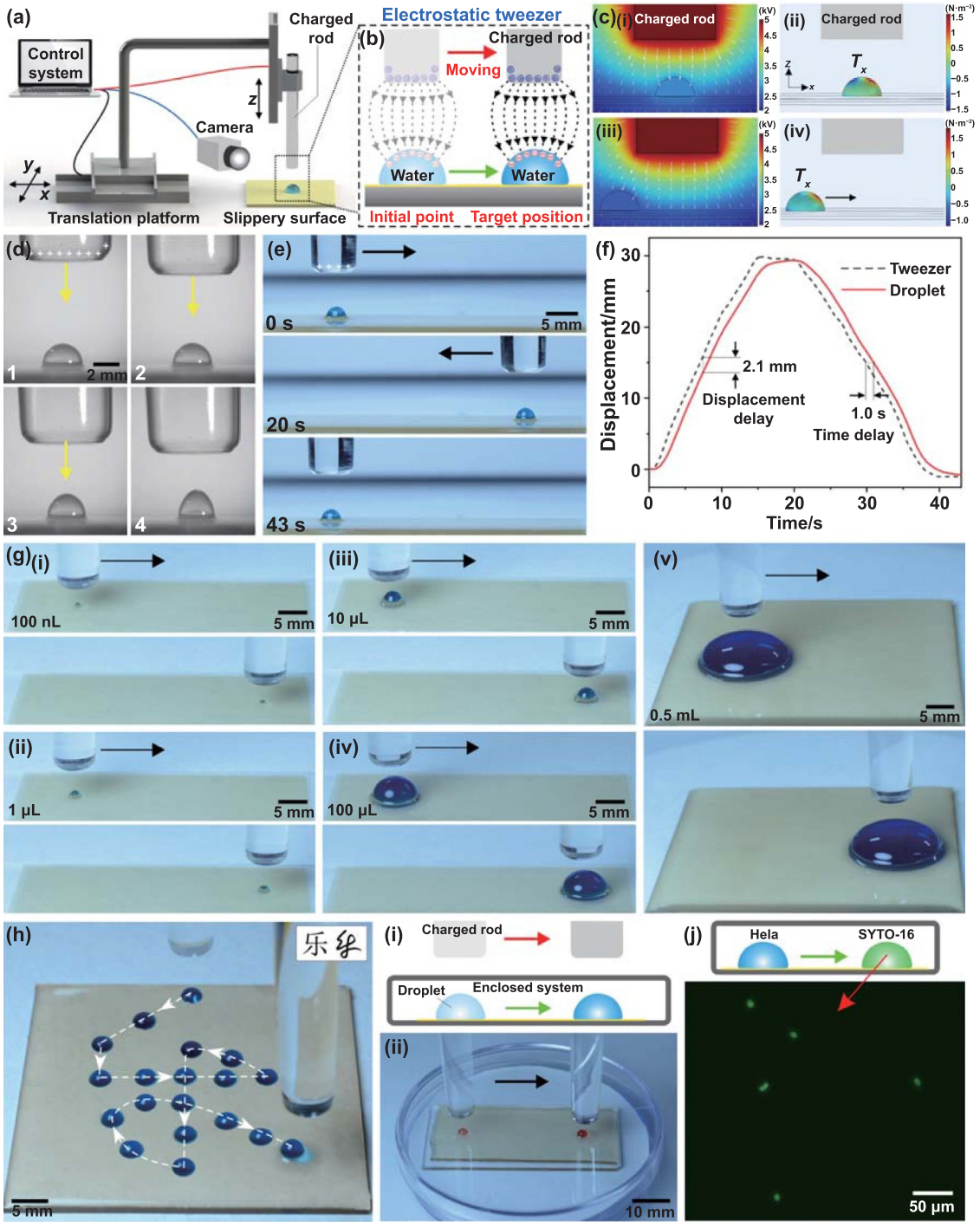

Figure 5. Mechanically assisted vertical electrostatic tweezers for precise droplet manipulation. (a) Schematic of the mechanically assisted VET method with a TCR assembled vertically on a three-dimensional mobile platform. (b) Schematic of moving a droplet on a slippery surface with a VET. (c) Mechanism of the ability of the VET to trap and move droplets: (i) and (iii) numerical simulation of the electric potential distribution around the TCR with a surface polarization voltage of +5 kV (white arrows indicating the direction and magnitude of the electric field strength) and (ii) and (iv) the distribution of the Maxwell stress tensor exerted on the droplet in the lateral direction (T_x). The distribution of the Maxwell stress tensor in the vertical direction (T_z) is shown in figure S14 in the supporting information. (d) The shape change of a droplet with decreasing distance between the vertical TCR and the droplet. (e) Manipulating a droplet back and forth on the slippery surface by moving the TCR horizontally. (f) Position delay between the droplet and the rod when the droplet is moving. (g) Using the VET to manipulate droplets of different volumes: (i) 100 nl, (ii) 1 μl, (iii) 10 μl, (iv) 100 μl, and (v) 0.5 ml. (h) Using the VET to guide a water droplet to move along a track shaped like a handwritten Chinese character (meaning 'happy'). The insets are the printed form (left) and the author's signature (right) of this Chinese character. (i) Remote manipulation of liquids in an enclosed system by an external VET: (i) schematic of the operation process and (ii) optical time-lapse trajectory of the motion of the droplet in an enclosed Petri dish. (j) Cell staining and corresponding fluorescence image in an enclosed system. The droplet containing HeLa cells was moved to contact with the SYTO-16 droplet to label the nucleus with green fluorescence.

The noncontact manipulation of droplets in an enclosed system from the outside is difficult to achieve via other methods. In some special applications, such as biomedicine, the remote operation of liquids in enclosed systems is highly useful. For example, figure 5(j) shows a simple cell labeling experiment in which the VET manipulates a droplet containing HeLa cells to merge with a PBS aqueous droplet containing SYTO-16 stain to stain the cell nucleus in an enclosed Petri dish. The cells were labeled with green fluorescence without opening the culture system. In this process of manipulating cells, the closed space ensures that the cells are not polluted by the external environment and that the gaseous environment of the cell culture is not changed. TETs provide a low-cost, contactless, highly controllable, and portable way to move and merge droplets isolated from the external environment.

3. Conclusions

In conclusion, TETs are used to achieve contactless, flexible, and precise droplet manipulation on lubricated slippery surfaces prepared by femtosecond laser processing, which has many advantages over electrostatic droplet manipulation on superhydrophobic surfaces (table 1). Under the influence of the electrostatic field generated by the TCR, the positive and negative charges inside the droplet are redistributed, allowing the droplet to move under the action of electrostatic forces. The features of slippery surfaces endow TETs with diverse working conditions and functions. For example, a TET can drive a droplet to climb an inclined surface and even move suspended droplets on an inverted/upright surface. Droplets with different volumes (from 100 nl to 0.5 ml), chemical compositions, and surface tensions can be manipulated on the as-prepared slippery surface. Even corrosive HCl acid, NaOH alkali, NaCl salt solutions, and ethanol with a surface tension of only 22.3 $mN{\cdot}m^{-1}$ can be manipulated by electrostatic interactions. This manipulation is also suitable for small bubbles and solid balls. The flexibility of liquids allows droplets to be driven to pass through a narrow slit. The electrostatic force can also attract droplets to slide over damaged areas because of the inherent self-repairing ability of slippery surfaces. TETs can support a wide range of droplet-related applications, such as motion guidance, motion switching, droplet-based microreaction, surface cleaning, surface defogging, and liquid sorting. In particular, a TET can even manipulate droplets in an enclosed system. A simple cell labeling experiment was successfully performed by means of the TET without opening the culture system.

TET is a powerful tool for manipulating liquids and has many unique functions that cannot be compared with those of other droplet-manipulation methods (whether active or passive). We believe that the combination of TET with slippery surfaces will lead to exciting applications ranging from biological analysis to chemical manufacturing and from microfluidics to intelligent printing.

4. Experimental section

4.1. Materials

Solid PDMS was prepared by mixing the Sylgard 184 liquid prepolymer (Dow Corning Corporation) and its curing agent at a volume ratio of 10:1. The mixture was then poured on a glass substrate, followed by heating at 80 °C for 4 h. As a result, cured PDMS sheets with a thickness of 1 mm were adhered to the glass substrates. The glass rods, rubber rods, silks, and furs used to generate static electricity by friction were purchased from online stores. PTFE and aluminum substrates were purchased from YuanDongLi Internet Corporation. Silicon wafers were purchased from SILICON WAFER Corporation. The glass substrates used were ordinary microscope slides (CITOTEST). Silicone oil (PMX-200, 10 cSt) was purchased from Dow Corning. Pure milk, coffee, Coca-Cola, and orange juice were purchased from a local supermarket. HCl, NaOH, NaCl, ethanediol, propanediol, ethanol, $AgNO_3$, $FeCl_3$, and phenol were purchased from Sinopharm Chemical Reagent Co., Ltd. Deionized water was used as the main measured liquid droplet.

4.2. Preparation of the superhydrophobic surface and lubricated slippery surface

A femtosecond laser (Spectra-Physics, USA) was used to generate the required microstructure on the PDMS surface. As shown in figure S2 (supporting information), the laser pulses (pulse duration = 75 fs, central wavelength = 800 nm, repetition rate = 1 kHz, pulse energy = 500 μJ) were guided into a high-speed galvanometer scanner (s-9210d, Sunny Technology, China) and further focused onto the PDMS surface by an f–θ lens (focal length = 160 mm) with a spot diameter of $\sim$30 μm. The laser scanning speed and scanning space were set at 10 $mm{\cdot}s^{-1}$ and 30 μm, respectively, under line-by-line scanning. The laser-treated samples were carefully cleaned with ethanol and deionized water under ultrasonication. The laser-structured PDMS surface directly exhibited superhydrophobicity. To obtain a lubricated slippery surface, silicone oil was used as the lubricant and poured onto the sample surface, allowing the silicone oil to fill the rough microstructures of the PDMS surface. Excess oil was removed by standing the sample upright. The method for preparing superhydrophobic and slippery surfaces on PTFE, aluminum, silicon, and glass substrates is similar to the above process, except that the laser-treated aluminum, silicon, and glass surfaces require a low-surface-energy modification.

4.3. Electrostatic droplet manipulation

A glass rod with a diameter of approximately 7 mm was positively charged by rubbing it against the silk. Similarly, a rubber rod was negatively charged by rubbing it against the fur. The electrostatic potential on the surface of the charged rod was measured by an electrostatic voltage tester (FMX-003, Xiangruide Corp.). The induced electrostatic potential can be

adjusted (0 $\sim$ ($\pm$6) kV) by the strength and speed of friction. The charged rod was moved close to the droplet until the droplet began to move. Unless otherwise specified, the volume of droplets used to achieve manipulation was 10 μl. The charged rod was then moved to guide the droplet forward, and the droplet was kept at a suitable distance from the charged rod.

4.4. ETs

The charged rod with frictional static electricity was vertically fixed on a three-dimensional mobile platform. The rod was first moved to the position above the droplet. Then, the height was decreased to a suitable height so that the charged rod could exert a strong binding force on the droplet. Through the movement of the mobile platform, the droplet moves with the rod and stays below the charged rod.

4.5. Cell culture and labeling

HeLa cells were grown in cell culture medium (Process, China) at 37 °C and 5% CO_2. When the cells reached 90% confluence, they were washed, treated with trypsin, centrifuged, and resuspended to produce a cell suspension. Then, a droplet containing the HeLa cells was transferred to the enclosed system (i.e. a closed Petri dish). The droplet was remotely moved to merge with another aqueous PBS droplet containing 2 μl·ml^{-1} SYTO-16 (KeyGEN, KGA260) for 30 min to stain the cell nucleus. After this, the fluorescence images of the droplets were observed by a fluorescence microscope (Leica, DMI8).

4.6. Electrostatic field simulation

Finite element analysis (COMSOL Multiphysics, MA, USA) was used to calculate the surface potential, electric field, and electrostatic force for droplet manipulation. In the simulation setup, electrostatic field physics was used in an air environment. The physical characteristics of the shapes and dimensions of the charged rod and the liquid droplet, as well as the initial surface potential, were chosen as in the measured experiments. The droplet deformation was small and therefore negligible in our simulations.

4.7. Other characterization

The surface microstructure of the PDMS substrates after femtosecond laser ablation was observed by a scanning electron microscope (GeminiSEM 500, Carl Zeiss). The wettability of the as-prepared superhydrophobic surface and slippery surface was measured by a contact-angle instrument (CA100C, Innuo). A digital camera (D7100, Nikon) was used to record the processes of electrostatic droplet manipulation. In particular, extremely fast droplet motions were captured by a high-speed camera (Chronos 2.1-HD, Kron Technologies) at 1000 fps.

Acknowledgments

This work was supported by the USTC Research Funds of the Double First-Class Initiative (Nos. YD2090002013, YD234000009) and the National Natural Science Foundation of China (Nos. 61927814, 62325507, 52122511, U20A20290, 62005262). We acknowledge the Experimental Center of Engineering and Material Sciences at USTC for the fabrication and measurement of the samples. This work was partly carried out at the USTC Center for Micro and Nanoscale Research and Fabrication.

Conflict of interest

There are no conflicts to declare.

ORCID iDs

Jiale Yong https://orcid.org/0000-0003-2144-7330
Dong Wu https://orcid.org/0000-0003-0623-1515

References

[1] Hajji I, Serra M, Geremie L, Ferrante I, Renault R, Viovy J L, Descroix S and Ferraro D 2020 Droplet microfluidic platform for fast and continuous-flow RT-qPCR analysis devoted to cancer diagnosis application *Sens. Actuators* B **303** 127171
[2] Song J, Cheng W F, Nie M T, He X K, Nam W, Cheng J T and Zhou W 2020 Partial Leidenfrost evaporation-assisted ultrasensitive surface-enhanced Raman spectroscopy in a Janus water droplet on hierarchical plasmonic micro-/nanostructures *ACS Nano* **14** 9521–31
[3] Zhang S P *et al* 2018 Digital acoustofluidics enables contactless and programmable liquid handling *Nat. Commun.* **9** 2928
[4] Abdelgawad M and Wheeler A R 2009 The digital revolution: a new paradigm for microfluidics *Adv. Mater.* **21** 920–5
[5] Seemann R, Brinkmann M, Pfohl T and Herminghaus S 2012 Droplet based microfluidics *Rep. Prog. Phys.* **75** 016601
[6] Wu D *et al* 2020 High-performance unidirectional manipulation of microdroplets by horizontal vibration on femtosecond laser-induced slant microwall arrays *Adv. Mater.* **32** 2005039
[7] Bai X, Yang Q, Fang Y, Yong J L, Bai Y K, Zhang J W, Hou X and Chen F 2020 Anisotropic, adhesion-switchable, and thermal-responsive superhydrophobicity on the femtosecond laser-structured shape-memory polymer for droplet manipulation *Chem. Eng. J.* **400** 125930
[8] Jiang M N *et al* 2022 Inhibiting the Leidenfrost effect above 1,000 °C for sustained thermal cooling *Nature* **601** 568–72
[9] Vorobyev A Y and Guo C L 2009 Metal pumps liquid uphill *Appl. Phys. Lett.* **94** 224102
[10] Zheng Y M, Bai H, Huang Z B, Tian X L, Nie F Q, Zhao Y, Zhai J and Jiang L 2010 Directional water collection on wetted spider silk *Nature* **463** 640–3
[11] Zhang S N, Huang J Y, Chen Z and Lai Y K 2017 Bioinspired special wettability surfaces: from fundamental research to water harvesting applications *Small* **13** 1602992
[12] Dong Z C, Ma J and Jiang L 2013 Manipulating and dispensing micro/nanoliter droplets by superhydrophobic needle nozzles *ACS Nano* **7** 10371–9

[13] Jokinen V, Sainiemi L and Franssila S 2008 Complex droplets on chemically modified silicon nanograss *Adv. Mater.* **20** 3453–6
[14] Xu J K, Xiu S, Lian Z X, Yu H D and Cao J J 2022 Bioinspired materials for droplet manipulation: principles, methods and applications *Droplet* **1** 11–37
[15] Tang Q, Liu X F, Cui X X, Su Z P, Zheng H, Tang J and Joo S W 2021 Contactless discharge-driven droplet motion on a nonslippery polymer surface *Langmuir* **37** 14697–702
[16] Hernández S C *et al* 2013 Chemical gradients on graphene to drive droplet motion *ACS Nano* **7** 4746–55
[17] Yu C M, Cao M Y, Dong Z C, Wang J M, Li K and Jiang L 2016 Spontaneous and directional transportation of gas bubbles on superhydrophobic cones *Adv. Funct. Mater.* **26** 3236–43
[18] Ma H Y, Cao M Y, Zhang C H, Bei Z L, Li K, Yu C M and Jiang L 2018 Directional and continuous transport of gas bubbles on superaerophilic geometry-gradient surfaces in aqueous environments *Adv. Funct. Mater.* **28** 1705091
[19] Xiao X, Zhang C H, Ma H Y, Zhang Y H, Liu G L, Cao M Y, Yu C M and Jiang L 2019 Bioinspired slippery cone for controllable manipulation of gas bubbles in low-surface-tension environment *ACS Nano* **13** 4083–90
[20] Sun Q *et al* 2019 Surface charge printing for programmed droplet transport *Nat. Mater.* **18** 936–41
[21] Yong J L, Peng Y B, Wang X W, Li J W, Hu Y L, Chu J R and Wu D 2023 Self-driving underwater "aerofluidics" *Adv. Sci.* **10** 2301175
[22] Demirörs A F, Aykut S, Ganzeboom S, Meier Y A and Poloni E 2021 Programmable droplet manipulation and wetting with soft magnetic carpets *Proc. Natl Acad. Sci. USA* **118** e2111291118
[23] Han K and Yong K 2021 Overcoming limitations in surface geometry-driven bubble transport: bidirectional and unrestricted movement of an underwater gas bubble using a magnetocontrollable nonwetting surface *Adv. Funct. Mater.* **31** 2101970
[24] Wang J, Zhu Z X, Liu P F, Yi S Z, Peng L L, Yang Z L, Tian X L and Jiang L L 2021 Magneto-responsive shutter for on-demand droplet manipulation *Adv. Sci.* **8** 2103182
[25] Jin Y K, Wu C Y, Sun P C, Wang M M, Cui M M, Zhang C and Wang Z K 2022 Electrification of water: from basics to applications *Droplet* **1** 92–109
[26] Li W, Tang X and Wang L Q 2020 Photopyroelectric microfluidics *Sci. Adv.* **6** eabc1693
[27] Wang F, Liu M J, Liu C, Zhao Q L, Wang T, Wang Z K and Du X M 2022 Light-induced charged slippery surfaces *Sci. Adv.* **8** eabp9369
[28] Yuan Z C, Lu C G, Liu C, Bai X G, Zhao L, Feng S L and Liu Y H 2023 Ultrasonic tweezer for multifunctional droplet manipulation *Sci. Adv.* **9** eadg2352
[29] Hong X, Gao X F and Jiang L 2007 Application of superhydrophobic surface with high adhesive force in no lost transport of superparamagnetic microdroplet *J. Am. Chem. Soc.* **129** 1478–9
[30] Zhu S W *et al* 2020 High performance bubble manipulation on ferrofluid-infused laser-ablated microstructured surfaces *Nano Lett.* **20** 5513–21
[31] Jiang S J *et al* 2020 Three-dimensional multifunctional magnetically responsive liquid manipulator fabricated by femtosecond laser writing and soft transfer *Nano Lett.* **20** 7519–29
[32] Ben S, Ning Y Z, Zhao Z H, Li Q, Zhang X D, Jiang L and Liu K S 2022 Underwater directional and continuous manipulation of gas bubbles on superaerophobic magnetically responsive microcilia array *Adv. Funct. Mater.* **32** 2113374
[33] Shao K X, Jiang S J, Hu Y L, Zhang Y Y, Li C Z, Zhang Y X, Li J W, Wu D and Chu J R 2022 Bioinspired lubricated slippery magnetic responsive microplate array for high performance multi-substance transport *Adv. Funct. Mater.* **32** 2205831
[34] van der Heyden F H J, Stein D and Dekker C 2005 Streaming currents in a single nanofluidic channel *Phys. Rev. Lett.* **95** 116104
[35] van der Heyden F H J, Bonthuis D J, Stein D, Meyer C and Dekker C 2006 Electrokinetic energy conversion efficiency in nanofluidic channels *Nano Lett.* **6** 2232–7
[36] Dai H Y, Gao C, Sun J H, Li C X, Li N, Wu L, Dong Z C and Jiang L 2019 Controllable high-speed electrostatic manipulation of water droplets on a superhydrophobic surface *Adv. Mater.* **31** 1905449
[37] Jin Y K, Xu W H, Zhang H H, Li R R, Sun J, Yang S Y, Liu M J, Mao H Y and Wang Z K 2022 Electrostatic tweezer for droplet manipulation *Proc. Natl Acad. Sci. USA* **119** e2105459119
[38] Wang D H *et al* 2020 Design of robust superhydrophobic surfaces *Nature* **582** 55–59
[39] Yong J L, Huo J L, Yang Q, Chen F, Fang Y, Wu X J, Liu L, Lu X Y, Zhang J Z and Hou X 2018 Femtosecond laser direct writing of porous network microstructures for fabricating super-slippery surfaces with excellent liquid repellence and anti-cell proliferation *Adv. Mater. Interfaces* **5** 1701479
[40] Wong T S, Kang S H, Tang S K Y, Smythe E J, Hatton B D, Grinthal A and Aizenberg J 2011 Bioinspired self-repairing slippery surfaces with pressure-stable omniphobicity *Nature* **477** 443–7
[41] Yong J L, Chen F, Yang Q, Fang Y, Huo J L, Zhang J Z and Hou X 2017 *Nepenthes* inspired design of self-repairing omniphobic slippery liquid infused porous surface (SLIPS) by femtosecond laser direct writing *Adv. Mater. Interfaces* **4** 1700552
[42] Cheng Y *et al* 2023 Heart valve-inspired self-lubricating anticoagulant surfaces *Chem. Eng. J.* **474** 145358
[43] Zhang J L, Yang Q, Cheng Y, Fang Z, Hou X and Chen F 2022 Slippery liquid-infused porous surface on metal material with excellent ice resistance fabricated by femtosecond Bessel laser *Adv. Eng. Mater.* **24** 2101738
[44] Liang J, Shan C, Wang H, Hu T, Yang Q, Li H Y, Hou X and Chen F 2022 Highly stable and transparent slippery surface on silica glass fabricated by femtosecond laser *Adv. Eng. Mater.* **24** 2200708
[45] Wang Q, Zhang Y C, Sun H B, Zou W K, Miao N D, Liu S L, Jiao Y H, Liu Y Q and Han D D 2023 Laser-induced graphene for slippery photothermal de-icing surfaces *IEEE Photonics Technol. Lett.* **35** 1167–70
[46] Han D D, Zhang Y L, Chen Z D, Li J C, Ma J N, Mao J W, Zhou H and Sun H B 2023 Carnivorous plants inspired shape-morphing slippery surfaces *Opto-Electron. Adv.* **6** 210163
[47] Jiao Z Z, Zhou H, Han X C, Han D D and Zhang Y L 2023 Photothermal responsive slippery surfaces based on laser-structured graphene@PVDF composites *J. Colloid Interface Sci.* **629** 582–92
[48] Yong J L, Yang Q, Hou X and Chen F 2022 Nature-inspired superwettability achieved by femtosecond lasers *Ultrafast Sci.* **2022** 9895418
[49] Yong J L, Yang Q, Huo J L, Hou X and Chen F 2022 Underwater gas self-transportation along femtosecond laser-written open superhydrophobic surface microchannels ($<$100 μm) for bubble/gas manipulation *Int. J. Extrem. Manuf.* **4** 015002
[50] Zhang Y X, Wu D, Zhang Y C, Bian Y C, Wang C W, Li J W, Chu J R and Hu Y L 2023 Femtosecond laser direct writing of functional stimulus-responsive structures and applications *Int. J. Extrem. Manuf.* **5** 042012

[51] Zhu L, Zhang Y L and Sun H B 2021 Miniaturising artificial compound eyes based on advanced micronanofabrication techniques *Light* **2** 84–100
[52] Zhang D S, Li X Z, Fu Y, Yao Q H, Li Z G and Sugioka K 2022 Liquid vortexes and flows induced by femtosecond laser ablation in liquid governing formation of circular and crisscross LIPSS *Opto-Electron. Adv.* **5** 210066
[53] Mao J W, Han D D, Zhou H, Sun H B and Zhang Y L 2023 Bioinspired superhydrophobic swimming robots with embedded microfluidic networks and photothermal switch for controllable *Marangoni* propulsion *Adv. Funct. Mater.* **33** 2208677
[54] Wang H, Zhang Y L, Han D D, Wang W and Sun H B 2021 Laser fabrication of modular superhydrophobic chips for reconfigurable assembly and self-propelled droplet manipulation *PhotoniX* **2** 17
[55] Cassie A B D and Baxter S 1944 Wettability of porous surfaces *Trans. Faraday Soc.* **40** 546–51
[56] Wang S and Jiang L 2007 Definition of superhydrophobic states *Adv. Mater.* **19** 3423–4
[57] Yong J L, Chen F, Yang Q, Huo J L and Hou X 2017 Superoleophobic surfaces *Chem. Soc. Rev.* **46** 4168–217
[58] Li M J, Yang T Z, Yang Q, Fang Z, Bian H, Zhang C J, Hou X and Chen F 2022 Bioinspired anti-fogging and anti-fouling artificial compound eyes *Adv. Opt. Mater.* **10** 2200861
[59] Yu C M, Zhu X B, Li K, Cao M Y and Jiang L 2017 Manipulating bubbles in aqueous environment via a lubricant-infused slippery surface *Adv. Funct. Mater.* **27** 1701605
[60] Ristenpart W D, Bird J C, Belmonte A, Dollar F and Stone H A 2009 Non-coalescence of oppositely charged drops *Nature* **461** 377–80
[61] Li N, Wu L, Yu C L, Dai H Y, Wang T, Dong Z C and Jiang L 2018 Ballistic jumping drops on superhydrophobic surfaces via electrostatic manipulation *Adv. Mater.* **30** 1703838
[62] Han X, Tan S D, Jin R Y, Jiang L and Heng L P 2023 Noncontact charge shielding knife for liquid microfluidics *J. Am. Chem. Soc.* **145** 6420–7
[63] Wang F X, Guo F Z, Wang Z Q, He H L, Sun Y, Liang W Y and Yang B 2022 Surface charge density gradient printing to drive droplet transport: a numerical study *Langmuir* **38** 13697–706
[64] Link D R, Grasland-mongrain E, Duri A, Sarrazin F, Cheng Z D, Cristobal G, Marquez M and Weitz D A 2006 Electric control of droplets in microfluidic devices *Angew. Chem., Int. Ed.* **45** 2556–60
[65] Jin Y K *et al* 2023 Charge-powered electrotaxis for versatile droplet manipulation *ACS Nano* **17** 10713–20
[66] Xu W H, Jin Y K, Li W B, Song Y X, Gao S W, Zhang B P, Wang L L, Cui M M, Yan X T and Wang Z K 2022 Triboelectric wetting for continuous droplet transport *Sci. Adv.* **8** eade2085
[67] Furmidge C G L 1962 Studies at phase interfaces. I. The sliding of liquid drops on solid surfaces and a theory for spray retention *J. Colloid Sci.* **17** 309–24
[68] Cao M Y, Jin X, Peng Y, Yu C M, Li K, Liu K S and Jiang L 2017 Unidirectional wetting properties on multi-bioinspired magnetocontrollable slippery microcillia *Adv. Mater.* **29** 1606869
[69] Daniel D, Timonen J V I, Li R P, Velling S J and Aizenberg J 2017 Oleoplaning droplets on lubricated surfaces *Nat. Phys.* **13** 1020–5
[70] Tang X, Li W and Wang L Q 2021 Furcated droplet motility on crystalline surfaces *Nat. Nanotechnol.* **16** 1106–12
[71] Keiser A, Baumli P, Vollmer D and Quéré D 2020 Universality of friction laws on liquid-infused materials *Phys. Rev. Fluids* **5** 014005
[72] Yan W H, Xue S Y, Xiang B, Zhao X R, Zhang W, Mu P and Li J 2023 Recent advances of slippery liquid-infused porous surfaces with anti-corrosion *Chem. Commun.* **59** 2182–98
[73] Lv P, Zhang Y L, Han D D and Sun H B 2021 Directional droplet transport on functional surfaces with superwettabilities *Adv. Mater. Interfaces* **8** 2100043
[74] Zhang X D, Ben S, Zhao Z H, Ning Y Z, Li Q, Long Z Y, Yu C M, Liu K S and Jiang L 2023 Lossless and directional transport of droplets on multi-bioinspired superwetting V-shape rails *Adv. Funct. Mater.* **33** 2212217